MDPI

Article

An Oil Wear Particles Inline Optical Sensor Based on Motion Characteristics for Rotating Machines Condition Monitoring

Zhenzhen Liu [1], Yan Liu [1,*], Hongfu Zuo [1], Han Wang [1,2] and Zhixiong Chen [3]

[1] Civil Aviation Key Laboratory of Aircraft Health Monitoring and Intelligent Maintenance, College of Civil Aviation, Nanjing University of Aeronautics and Astronautics, Nanjing 211100, China

[2] Center for Advanced Life Cycle Engineering, Department of Mechanical Engineering, University of Maryland, College Park, MD 20740, USA

[3] School of Air Transport, Shanghai University of Engineering Science, Shanghai 201620, China

* Correspondence: jiayinly@nuaa.edu.cn

Abstract: Since inline monitoring method has the advantages of no sampling, being real-time, no human intervention, and low error, this paper innovatively proposes to study the inline monitoring of wear particles in an oil pipeline, from the perspective of the different motion characteristics of the particles. In this paper, an inline optical sensor was designed and developed by studying the velocity characteristics of different particles through theoretical calculations, numerical simulations, and experimental analysis. First, an equation for particle motion was statistically established, based on the forces acting on wear particles in an oil-filled vertical tube. Then a finite element model of particle motion in a full-flow oil pipeline was created, to simulate particle motion with various diameters, densities, locations, and shapes. Finally, the results of the theoretical study were effectively applied to design an inline optical monitoring sensor, and the experimental validation results demonstrated that the inline sensor has excellent suitability for monitoring wear particles. This study has significance for the safe operation of large rotating machinery.

Keywords: oil particle; forces; properties; motion velocity; mathematical model

1. Introduction

After the outbreak of the global epidemic in 2019, there was a massive shortage of energy supply in the world, while the phenomenon of friction with the presence of relative motion consumes one third of the world's available energy; therefore, green tribology is currently one of the most important development directions of tribology. Tribological wear is the main cause of material and mechanical equipment failure. Approximately 80% of machine parts fail due to friction, and over 50% of sever accidents involving mechanical equipment are caused by lubrication failure and excessive wear [1]. For large rotating machinery, bearings and gears are commonly used as key transmission components, and their fault diagnosis has been the focus of research in this field [2–8]. As these components need to be lubricated, oil is the blood of mechanical equipment. The wear particles in the oil carry multi-dimensional information for characterizing the health status of the equipment [9]. Consequently, it is extremely important to monitor the wear particles in oil.

According to tribological research, the type, number, and increase rate of wear particles are directly proportional to the degree of wear of the friction surface material. The density, color, and size of particles are closely related to the type and process of wear [10]. Thus, monitoring the properties of wear particles can play a significant role in determining the location, severity, developmental trends, and causes of wear faults. There are various electrostatic [11], capacitive [12], inductive [13], and optical [14] sensors for monitoring the properties of wear particles. However, with the rapid development of optical hardware technology and the higher sensitivity of optical sensors compared to other

technologies, there is growing research on the analysis of wear particles using optical techniques [15].

Offline ferrography [16–19] and online microfluidics [20,21] are common optical techniques for analyzing particles. Ferrography uses a high gradient magnetic field to separate metallic wear particles from lubricants and contaminants, to analyze the wear particle's state, size, composition, and formation mechanism. It is primarily utilized for the qualitative and quantitative analysis of ferromagnetic particles. However, the time cost of iron spectrum preparation is high, the wear particles tend to aggregate into chains on the spectrum, and wear debris images often suffer from image blurring, due to numerous noise sources [22,23]; thus, the results of the analysis of wear particles are highly dependent on the experience of the observer. At the same time, offline sensors are rapidly being phased out of the market, due to their poor timeliness. In addition, microfluidics is predominantly an online method, and online sensors also have a high error, due to sample monitoring. However, inline monitoring has the advantages of no sampling, being real-time, and no human intervention; as such, it has been rapidly developed over the past several years.

The movement of solid particles in liquids is a relatively classical problem in the discipline of fluid mechanics, and a great deal of research has been conducted on it. It is important to monitor solid particles in lubricating oil pipelines effectively. Moreover, particle flow is a widely occurring phenomenon in nature and industry, such as the spread of plant seeds, the diffusion of atmospheric pollutants, and the movement of particles in fluidized beds. Particle motion is influenced by certain variables, including disturbances in the external environment and interactions between particles. The behavior of individual particles has a significant impact on the behavior of multi-particle flows. Therefore, the study of the motion of individual particles is crucial to the further investigation of multi-particle motion in oil. Segré and Silberberg experimentally demonstrated that the radial position of a macroscopic rigid sphere moving in a Poiseuille fluid (laminar fluid in an infinitely long straight circular tube) is finally stabilized at the position of a circular region of 0.6-times the radius of the tube [24]. Jeffrey et al. investigated the motion of particles in a laminar vertical pipe experimentally and discovered that the motion of rigid spherical particles suspended in a viscous liquid was consistent with the Segre and Silberberg effect [25]. Huang et al. studied the motion of particles in an arbitrary flow field and found that the diameter and density of particles played an important role in the relative motion of liquid–solid two-phase flow; the larger the diameter and density of the particles, the greater the relative velocity of the two phases, and the effect of particle density is greater than the effect of particle diameter [26]. Choi et al. analyzed the influence of particles of different sizes, shapes, and densities on particle motion, using the PTV (particle tracking velocimetry) technique. The results showed that the relative velocities of liquids and solids were greater when the density difference was large [27]. Miura et al. established that the equilibrium location of a neutrally buoyant spherical particle moving between two parallel plates was governed by the particle's Reynolds number and the distance between the particle diameter and the two plates [28]. It is worth noting that the majority of the studies mentioned above on the motion of solid particles in liquids concentrated on the case of similar densities and small relative velocities or the motion of round spheres in unbounded fluids. In contrast, research on the combined motion of particles of different shapes and densities in fixed pipes is rare.

According to the above research, this paper innovatively proposed to study the inline monitoring of wear particles with different properties, from the perspective of the different motion characteristics of the particles. The objective was to identify the properties of various wear particles based on their different velocities, thus promoting the development of wear particles in lubricating oil inline monitoring technology and effectively preventing the occurrence of early failures. In this paper, an inline optical sensor was designed and developed by studying the velocity characteristics of different particles through theoretical calculations, numerical simulations, and experimental analysis. Consequently, gear and bearing wear can be quickly obtained using an optical sensor to inline monitor

the properties of wear particles in the oil pipeline. The research in this paper began with the force of the particles in the oil fluid and established equations of motion of simply shaped particles. Finite element models (FEM) of the particles with different properties were established in simulation software, and a multi-parameterized analysis was performed, to determine the motion law of the particles in the vertical pipe. Based on these results, a full-flow inline wear particle monitoring sensor was designed. Finally, the motion characteristics of different wear particles were experimentally verified on a pin-disk experimental machine, to establish a model for the motion monitoring of particles with different properties.

The rest of the paper is arranged as follows: Section 2 details the materials and methods, and Section 3 provides a detailed analysis of the results and discussion. Finally, the conclusions are given in Section 4.

2. Materials and methods

2.1. Framework

In large rotating machinery systems such as high-speed trains, civil aircraft, ships, and military aircraft, the important transmission components are lubricated and wear particles are present in the oil, due to the operation of the friction pairs (bearings, gears, etc.). Therefore, oil carrying wear particles could be used as a data source for this paper. This data then needed to be monitored in real-time, to ensure the normal operation of the various rotating machines over time. The oil was passed through self-developed inline monitoring sensors. In combination with the monitoring model and the basic parameters of the wear particles obtained by the tracking algorithm, the parameters of the wear properties were obtained, to determine the wear condition of the friction pair. If the monitored wear properties are greater than the monitoring threshold for the wear status of the equipment, a message is sent to an engineer. If the monitoring threshold is not exceeded, the monitoring continues. The monitoring model for the wear particles was derived from force analysis, numerical simulation, and experimental implementation, all of which corroborated each other. Force analysis was the first module. This was a mechanical analysis of a simplified solid particle in a liquid–solid two-phase flow, which gave the factors influencing the particle motion. The shape and density of the wear particles were then modelled parametrically in simulation software to analyze the laws. Finally, the laws were verified through experiments, and a kinematic monitoring model was summarized. A framework for monitoring the wear state of equipment using wear particles carried in oil is shown in Figure 1.
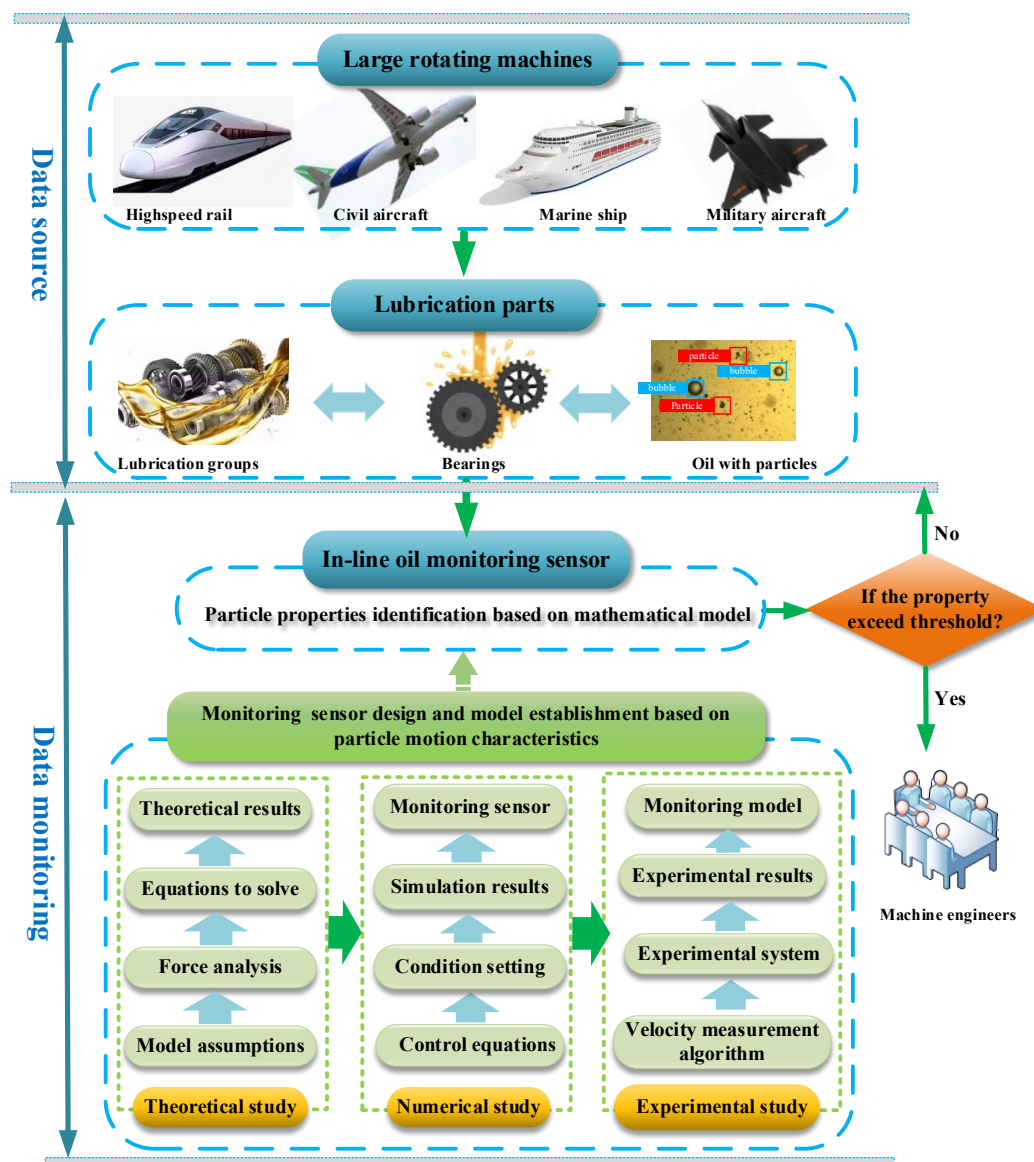
Figure 1. The proposed framework for analysis of the motion of wear particles.

2.2. Methods of Analyzing Wear Particle Motion

2.2.1. Theoretical Study

(a) Model assumptions

In order to obtain an inline monitoring model of particle properties, based on the movement characteristics of the particles in the oil, a force analysis of the particle's movement in the pipe was first required. It is well known that wear particles have various shapes, so the following assumptions were made to simplify the solution of the motion equations for the motion of particles in a pipe:

(1) Oil was stationary.
(2) Particles were rigid spherical particles.
(3) Oil was an incompressible viscous fluid.

(b) Force analysis of wear particle

The force environment of the model was analyzed following the BBO equation for particle motion in a viscous fluid by Oseen. [29] and the equation of motion for discrete particles in an arbitrary flow field by Huang et al. [26]: a solid particle of diameter d_P

and density ρ_p, placed in the tube cross-section at $z = 0$ (see Figure 2), at time $t = 0$. When $t > 0$, it started to move in the z-axis direction under gravity. The axial forces acting on the solid particle consist of:
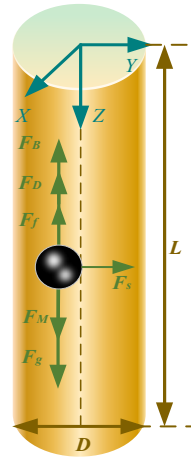

Figure 2. Diagram of the forces on a particle in a vertical pipe filled with oil.

$$F_g = \frac{1}{6}\pi d_p^{~3} \rho_p g \tag{1}$$

$$F_f = \frac{1}{6}\pi d_p^{~3} \rho_f g \tag{2}$$

$$F_D = \frac{1}{8}\pi \zeta d_p^{~2} \rho_f u_p^{~2} \tag{3}$$

$$F_M = \frac{1}{12}\pi d_p^{~3} \rho_f \frac{d(u_f - u_p)}{dt} \tag{4}$$

$$F_B = \frac{3}{2} d_p^{~2} \sqrt{\pi \rho_f \vartheta} \int_0^t \frac{d(u_f - u_p)/d\tau}{\sqrt{t - \tau}} d\tau \tag{5}$$

$$\zeta = \begin{cases} 24/Re_p, & Re_p \leq 2 \\ 18.5/Re_p^{~0.6}, & 2 < Re_p \leq 500 \\ 0.44, & Re_p > 500 \end{cases}, \quad Re_p = \frac{\rho_f d_p u_p}{\mu} \tag{6}$$

The radial forces on solid particles included:

$$F_s = 1.62 d_p^{~2} \sqrt{\rho_f \mu}(u_f - u_p)\sqrt{\left|\frac{du_f}{dy}\right|} \tag{7}$$

(c) Equations to solve

According to publications [30,31], particles with high densities are mainly affected by drag, gravitational, and buoyant forces. The Bassett and the Saffman lift forces are the next most important forces for medium density particles. However, it was experimentally verified in the paper [32] that the Bassett force accounts for less than 1% of the total force. At the same time, the oil considered in this study was stationary, so the Saffman lift could be neglected. In addition, the virtual mass force was negligible for almost all particles. Therefore, the mathematical model developed in this paper was:

$$\frac{\pi}{6}\rho_p d_p^{~3} \frac{du_p}{dt} = \frac{\pi}{6}\left(\rho_p - \rho_f\right)d_p^{~3} g - \frac{1}{8}\pi \zeta d_p^{~2} \rho_f u_p^{~2} \tag{8}$$

Given the initial condition $t = 0$, the $u_p = 0$

The equation was solved:

$$u_p = \begin{cases} \dfrac{d_p{}^2\left(\rho_p - \rho_f\right)g}{18\mu}, Re_p \leq 2 \\[3ex] 0.27\sqrt{\dfrac{d_p\left(\rho_p - \rho_f\right)g}{\rho_f}}\,Re_p{}^{0.6}, 2 < Re_p \leq 500 \\[3ex] 1.74\sqrt{\dfrac{d_p\left(\rho_p - \rho_f\right)g}{\rho_f}}, Re_p > 500 \end{cases} \tag{9}$$

It can be seen that the velocity of the particles after stabilization is closely related to their density, diameter, and viscosity, as well as the density of the oil, regardless of the fluid zone (laminar, transition, turbulent). This paper discusses the situation in the same oil, so only the variation in the properties of the wear particles was considered. The next step was to determine the fluid region associated with the actual size of the wear particles.

(d) Comparison of different properties of the particles

As shown in the wear process during the operation of equipment in Figure 3 [33], the particle's typical size in the oil was selected for analysis: the size range of wear particles is approximately 0.1~1000 μm. It can be seen that wear particles in the diameter range of 10–1000 μm should be monitored when the equipment increases wear. The difference in the trial method is used to determine whether the particles are moving in the laminar flow zone, the transition flow zone, or the turbulent flow zone. Assuming that the particles are settling in the laminar flow zone in the oil, the oil's viscosity is No. 26 hydraulic oil. Its viscosity is $0.02184\,\text{Pa}\cdot\text{s}$ at 20 °C, and the density is $840\,\text{kg/m}^3$. The particles are aluminum particles of diameter 1000 μm. The following is obtained according to the settling velocity formula in the laminar flow zone.

$$u_p = \frac{d_p{}^2\left(\rho_p - \rho_f\right)g}{18\mu} = \frac{\left(1\times10^{-3}\right)^2 \times \left(2700 - 840\right) \times 9.81}{18 \times 0.02184} = 0.0464\,\text{m/s} \tag{10}$$

Then

$$Re_p = \frac{\rho_f d_p u_p}{\mu} = \frac{840 \times 1 \times 10^{-3} \times 0.0464}{0.02184} = 1.784 < 2 \tag{11}$$

$$F_D = 3\pi\mu d_p\left(u_f - u_p\right) \tag{12}$$

Thus, the original assumption of a laminar flow zone was correct. The viscous forces of wear particles in the laminar flow region could be simplified [20].
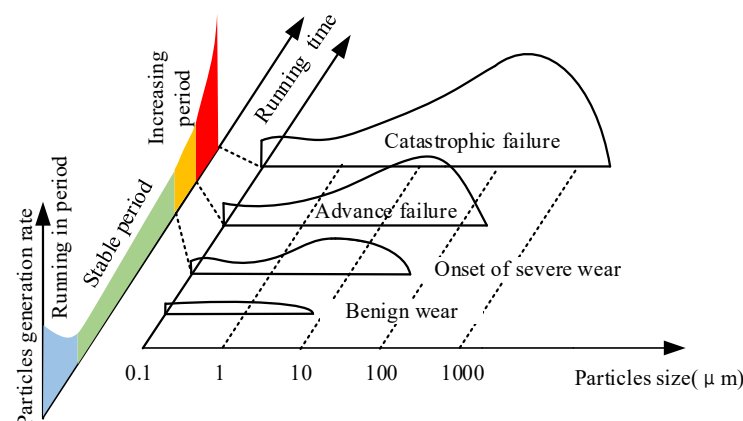

Figure 3. Relationship between debris generation and wear process.

The velocity trends of different densities and diameters of wear particles in oil with time are shown in Figure 4.
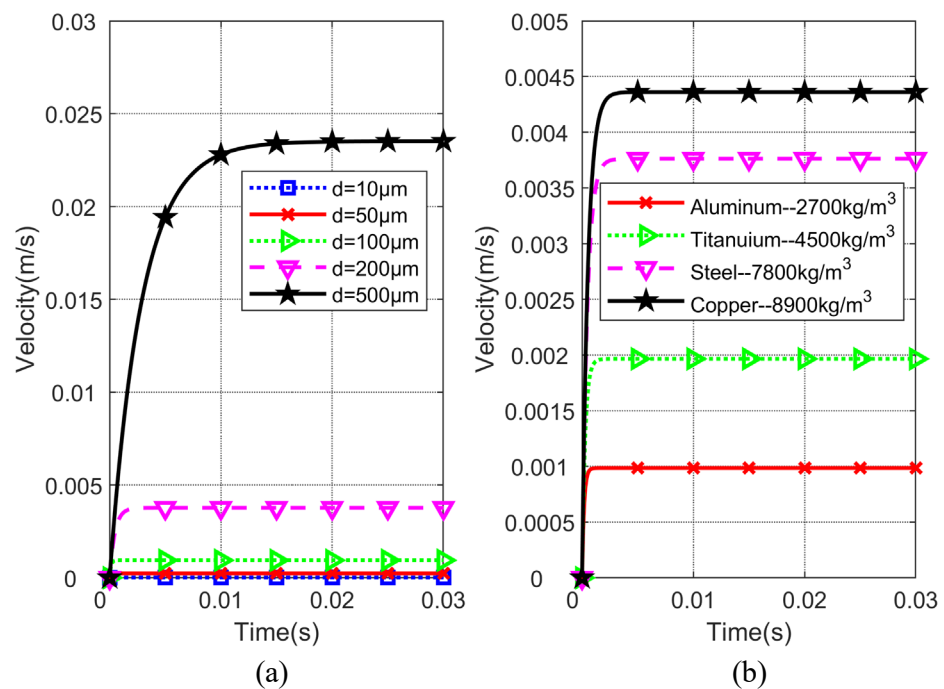

Figure 4. Velocities of particles with different properties moving in a vertical pipe: (**a**) iron particles of different diameters, (**b**) different density particles with a diameter of 200 μm.

2.2.2. Numerical Study

On the one hand, simulation of the movement characteristics of wear particles helps verify the theoretical analysis results. On the other hand, it can contribute to the design of the particle monitoring optical sensor in the next section and determine the installation position of the optical lens in the pipeline, to prevent particles from exceeding the lens's field of view and depth of field.

(a). Mathematical control equations

Numerical simulation is the process of using a computer to replace continuous physical quantities in time and space with a series of discrete particle changes and then establishing mathematical expressions or equations between these discrete particle variables, which are solved to obtain approximate values of the mass variables and display images of the calculated results. The fluid flow follows the conservation laws of momentum, mass, and energy. Since the heat change process during particle motion was not considered, the heat transfer equation was not analyzed.

The continuity equation expresses the law of conservation of mass in a fluid flow. When the fluid flows steadily, the equation is:

$$\frac{\partial\left(\rho_f u_x\right)}{\partial x}+\frac{\partial\left(\rho_f u_y\right)}{\partial y}+\frac{\partial\left(\rho_f u_z\right)}{\partial z}=0 \tag{13}$$

The motion equation is a specific expression of momentum conservation law in fluid flow. Since oil is an incompressible fluid, the simplified equation is:

$$\begin{cases} u_x \dfrac{\partial u_x}{\partial x} + u_y \dfrac{\partial u_x}{\partial y} + u_z \dfrac{\partial u_x}{\partial z} + \dfrac{\partial u_x}{\partial t} = f_x - \dfrac{1}{\rho_f} \dfrac{\partial p}{\partial x} + \nu \left(\dfrac{\partial^2 u_x}{\partial x^2} + \dfrac{\partial^2 u_x}{\partial y^2} + \dfrac{\partial^2 u_x}{\partial z^2} \right) \\[2ex] u_x \dfrac{\partial u_y}{\partial x} + u_y \dfrac{\partial u_y}{\partial y} + u_z \dfrac{\partial u_y}{\partial z} + \dfrac{\partial u_y}{\partial t} = f_y - \dfrac{1}{\rho_f} \dfrac{\partial p}{\partial y} + \nu \left(\dfrac{\partial^2 u_y}{\partial x^2} + \dfrac{\partial^2 u_y}{\partial y^2} + \dfrac{\partial^2 u_y}{\partial z^2} \right) \\[2ex] u_x \dfrac{\partial u_z}{\partial x} + u_y \dfrac{\partial u_z}{\partial y} + u_z \dfrac{\partial u_z}{\partial z} + \dfrac{\partial u_z}{\partial t} = f_z - \dfrac{1}{\rho_f} \dfrac{\partial p}{\partial z} + \nu \left(\dfrac{\partial^2 u_z}{\partial x^2} + \dfrac{\partial^2 u_z}{\partial y^2} + \dfrac{\partial^2 u_z}{\partial z^2} \right) \end{cases} \quad (14)$$

(b). Foundation of geometrical model and condition setting

Figure 5 depicts the entire modelling and simulation process, which included setting the model environment, creating geometric figures, setting material properties, defining physical boundary conditions, establishing meshes, running simulations, and post-processing results.
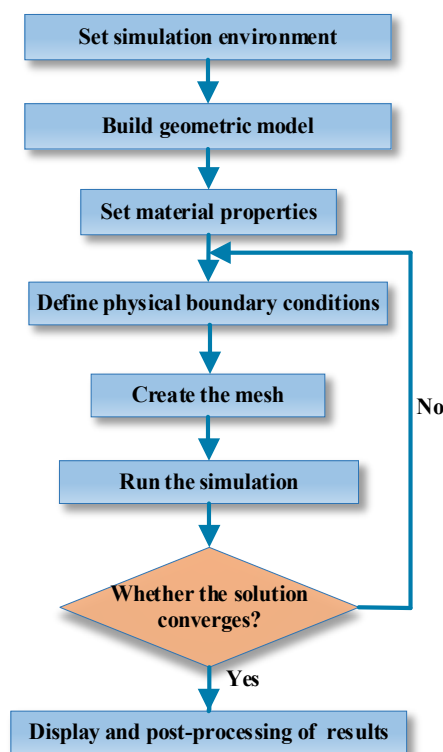

Figure 5. Calculation flowchart of the simulation.

The first step was to set up the model environment. The simulation of this model adopted two-dimensional geometry. The fluid flow employed a fluid–structure interaction module (the fluid–structure interaction module is required to simulate the motion law of relative macroscopic objects in the fluid, and the particle tracking module can be used when the particles are small, such as electrons and molecules), laminar flow, transient (field variables vary with time), Newtonian fluids, and liquid–solid two-phase flow.

Second, the geometry was established, and the geometry's size parameters and material properties were set. As illustrated in Figure 6 [34,35], the pipe diameter had a significant effect on the sedimentation velocity of the particles. As the ratio of particle diameter d_p to pipe diameter D grows, the effect of the pipe wall on particle's movement velocity becomes increasingly significant. Therefore, the wider the pipe diameter, the less the influence on the movement of the particles. Combined with the diameter of the conventional wear particles in Figure 2, ranging from 0.1 to 1000 μm, and the diameter of an actual common engine pipeline, the diameter of the round pipe was set to D = 8 mm, as well as combined with Figure 7, for the large density copper particles with a diameter of

1000 μm in oil, it takes about 0.14 s to reach the maximum stable speed of 0.2 m/s, and the maximum moving distance is still less than 30 mm; therefore, the pipe length *L* in the simulation model was set to 40 mm, to meet the moving distance of all particles in the system and to achieve a stable speed. In addition, the diameter of normal wear particles is less than 20 μm, and the wear of equipment can be determined by calculating the diameter and number of particles. Concerning shape, different wear mechanisms produce different shaped wear particles. When it comes to color, different wear areas are located in different places and produce different components of wear particles. Therefore, the diameter, shape, and density of the wear particles were used as parameters for analysis. In theoretical analysis, to qualitatively analyze the influencing factors of particle motion, the particles were reduced to spherical shapes. In the actual process, the shapes of the wear particles are mostly irregular flakes, blocks, strips, and regular spheres [36]. Therefore, this simulation took different shapes (round, triangular, rectangular) into account. At the same time, the three-dimensional model was simplified to a two-dimensional planar model, to simplify the model calculation. No. 26 industrial white oil with a viscosity of 0.022 Pa·s and a density of 850 kg/m³ was selected as the moving medium. The design of various detailed parameters of wear particles is shown in Table 1.
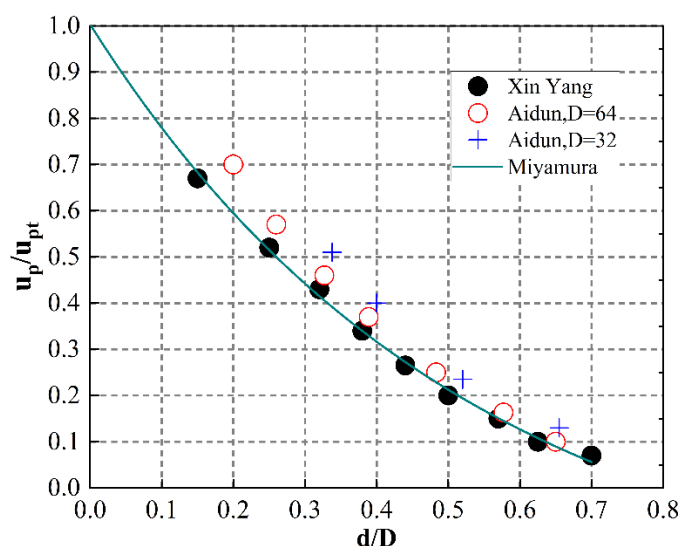

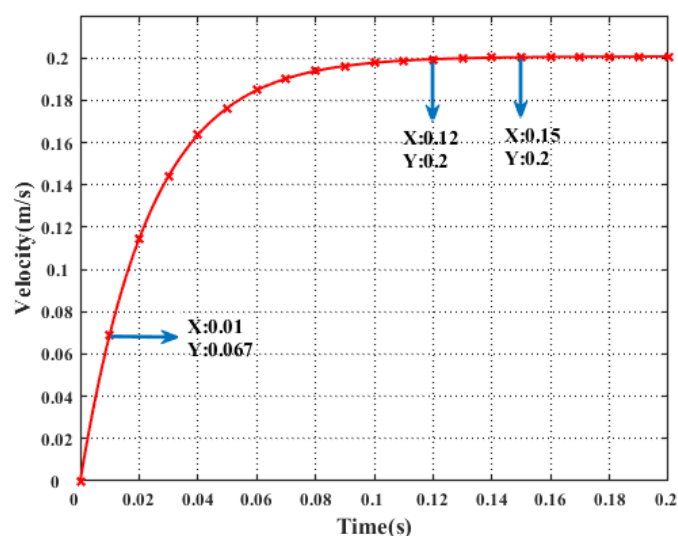**Figure 6.** Diagram of wall effect with the diameter.

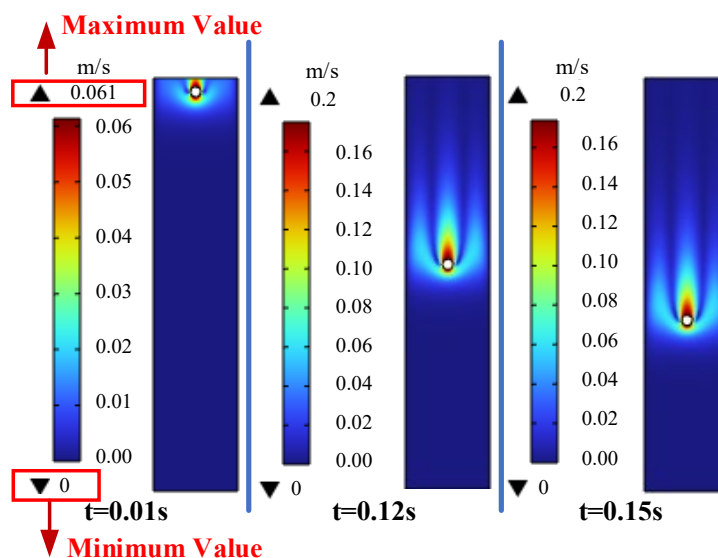**Figure 7.** Velocity of a copper particle with a diameter of 1000 μm.

Table 1. Particles for parametric sweeps.

Shape	Diameter (mm)	Density (kg/m³)	Material	Width (mm)	Height (mm)	Circularity
	1			/		1
	0.5	8960	copper	/		1
round	0.1			/		1
	0.5	4940	titanium	/		1
	0.5	2700	aluminum	/		1
triangle	/	8960	copper	1	1	0.6
square	/	8960	copper	1	0.2	0.5

Circularity = 4π * Area/Circumference².

The physical boundary conditions of the model were then defined, and the mesh was divided. Since the particle's initial velocity was zero, it settled down under the action of gravity, so the upper boundary was set as an open boundary. After the grid independence verification, it was found that the calculation performance was the highest when a finer grid was used. At the same time, automatic meshing was used in the solution process. The time step of the transient solution was set to 0.001 s, and the total solution time was 0.2 s.

Finally, the model was simulated, and the results were post-processed. In this paper, a parametric sweep was used to specify multi-dimensional parameters once, and the analysis results of different parameters were compared systematically, as shown in Figures 8–11.

Figure 8. Velocities of a copper particle with a diameter of 1 mm in the pipeline at different times.
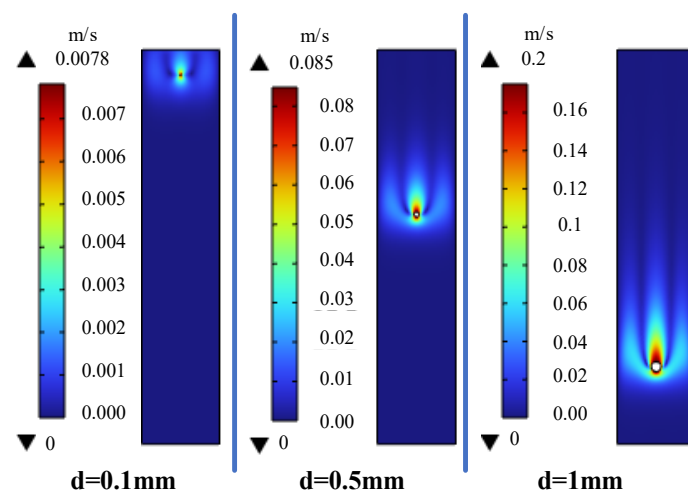
Figure 9. Velocities of copper particles with different diameters at t = 0.2 s.
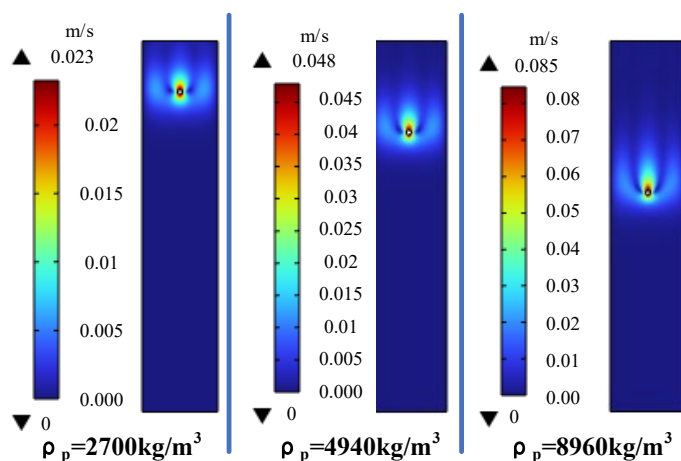
Figure 10. Velocities of 0.5 mm diameter particles with different densities at t = 0.2 s.
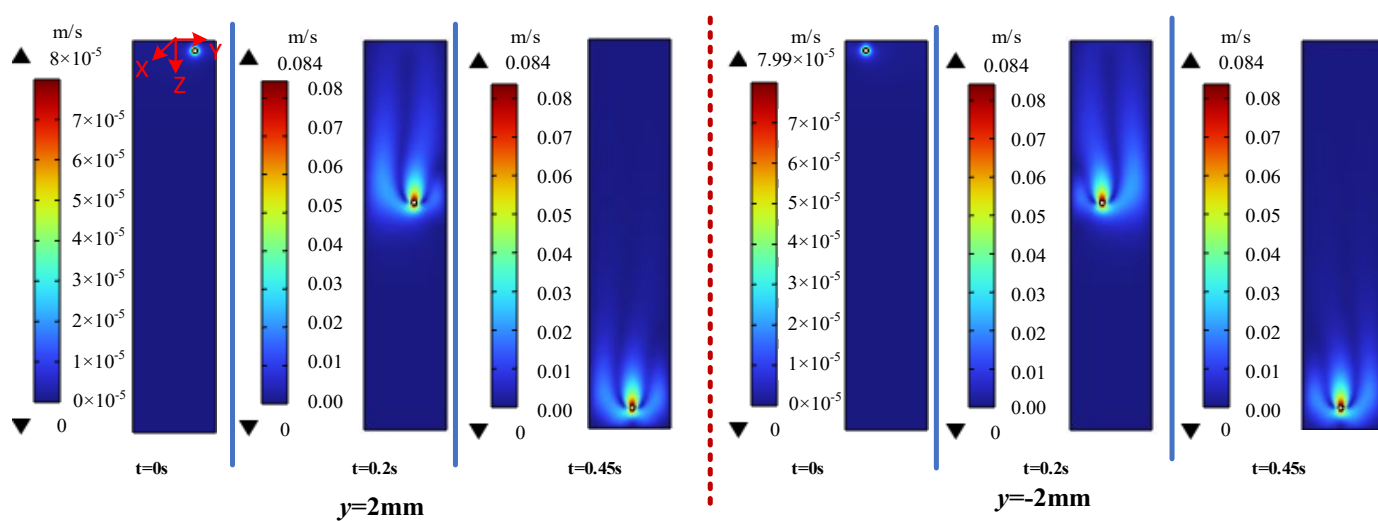
Figure 11. Velocities of 0.5 mm copper particle at different times after entering the pipeline from different positions (y = 2 mm, y = −2 mm).

3. Results and Discussion

3.1. Theoretical Study Results

Figure 4 demonstrates that the motion of a particle in a vertical pipe is divided into two periods, namely the acceleration period at the beginning and the uniform velocity period later. The reason for this is that when the particle begins to move, its initial velocity is zero, so the drag force is zero, and the acceleration is maximum. After the particle begins to move downwards in the vertical direction, the drag force increases as the particle velocity increases, and the acceleration decreases accordingly. When the velocity reaches a certain value, the drag force, buoyancy force, and gravity are in balance. The combined force on the particle is zero, making the acceleration zero. Then the particle's velocity no longer changes and performs a constant downward movement with velocity u_P. It is worth noting that the greater the particle density, the higher the final stable velocity, and the longer the time required to reach stability and the greater the distance covered. The larger the particle diameter, the higher the final steady velocity and the longer the time required to reach stability and the greater the distance covered. However, the time to reach steady-state velocity does not exceed 0.1 s in all cases. At the same time, the final velocity of the particles varies depending on their diameter and density, so the idea that the steady-state velocity of the particles can be used to distinguish the properties of the wear particles is correct.

3.2. Numerical Study Results

(a) Different times

Figure 8 shows the velocities of copper particles with a diameter of 1 mm in the pipeline at different times. It was found that it only takes a short time for the particle's velocity to go from zero to a constant. The theoretical simulation results in Figure 8 validate the theoretical analysis results in Figure 7 very well. However, there was a slight difference between the two at t = 0.01 s, because the theoretical analysis equation did not consider the influence of the pipe wall. Nevertheless, the speed of stability was highly consistent. This showed that the particles could reach a stable speed in a short time after entering the pipeline. We can directly consider the stabilization speed of the different property particles and ignore the accelerated stage at the beginning.

(b) Different diameters

Figure 9 depicts the velocities of three kinds of copper particles with diameters of 0.1 mm, 0.5 mm, and 1 mm after entering the pipe from the center of the pipe. It was found that after all the particles are released in the middle position, the particles hardly move in the horizontal direction during the descending process, and the particles settle vertically along the center line. The stable velocity of copper particle with a diameter of 1 mm was 0.2 m/s, which was consistent with the results in Figure 7, indicating that the simulation results were correct. In addition, the larger the particle diameter, the larger the final particle movement speed, and the particles hardly moved in the horizontal direction during the descending process. The particles settled vertically along the centerline. The entire flow field was symmetrical. The difference between the density of the particles and the fluid caused the particles to move in the direction of gravity. The drag force generated in the movement causes the fluid near the particle to move downward. At the same time, the fluid on both sides was squeezed during the particle's falling process, so that it had an upward velocity vector, thereby forming a vortex structure. With the increase of time, the particle's velocities gradually increased from zero and then reached a stable velocity under the action of the drag force. During this process, the vortex structure near the particle changed gradually. Finally, it formed two elongated vortex structures, due to the influence of the boundary. Moreover, the greater the particle's velocity, the greater the vortex.

(c) Different densities

Figure 10 displays the velocities of particles with a diameter of 0.5 mm and a density of 2700 kg/m^3, 4940 kg/m^3, and 8960 kg/m^3 entering the No. 26 oil from the center of the

pipeline. It was found that the greater the density of the particles, the greater the velocity needed to reach stabilization and the greater the distance travelled. Likewise, the particles had almost no movement in the horizontal direction during the descending process, the particles settled vertically along the centerline, and the entire flow field was symmetrical.

(d) Different locations

Figure 11 shows the velocities of 0.5-mm copper particles at different times after entering the pipeline from different positions ($y = 2$ mm, $y = -2$ mm). The particles gradually approached the axis of the pipeline as the time increased during the descending process. Moreover, the particles' velocities in the vertical direction were gradually increased. After the particles were released in symmetrical positions, their sedimentation trajectory was symmetrical around the centerline. In the y-direction, when the particle moved to the position of the centerline, the horizontal velocity was almost zero. The particles moved downward steadily in the vertical direction, and finally, the sedimentation velocity of the particles tended to become stable. Furthermore, the final velocity of the particles released from the eccentric position and the central position was the same, and this is consistent with the findings of Yang's study [34]. Therefore, the initial release position of the wear particles had no significant effect on the final velocity or the stabilization position in this pipe. The reason for this was that, under the action of gravity, the drag force drives the fluid near the particles downward and squeezes the fluids on both sides, to make them have an upward velocity vector, thus forming a vortex structure and making the particles finally descend along the axis of the pipe.

(e) Different shapes

Figure 12 shows the sedimentation motion of three different shapes of particles in the oil. It can be seen that the higher the circularity of the particles, the higher the falling speed after the particles have stabilized. The particles eventually descended steadily along the tube axis, and the vortices on both sides of the particles were symmetrical. Therefore, the force of the particles on both sides of the tube axis was also symmetrical.
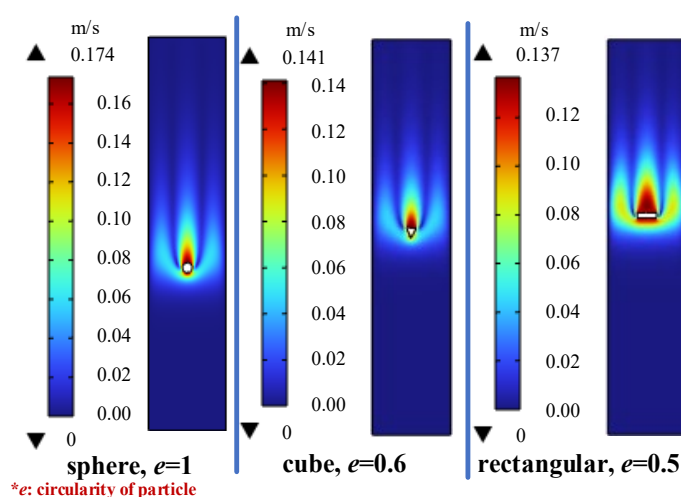

Figure 12. Velocities of particles with different shapes at t = 0.15 s.

Hence, the sedimentation state of the particles did not depend on the initial placement position of the particles, and the particle's stable velocity was influenced by its diameter, density, and circularity, regardless of where the particle entered the pipe. Consequently, the particle's properties could be judged by observing its velocity after stabilization.

3.3. Inline Monitoring Sensor Design

Based on the theoretical analysis results and simulation results of the movement laws of particles with different properties in the vertical pipeline, an inline monitoring sensor

for particles was designed. Its structure and diagram are shown in Figure 13. An LED surface light source was placed to capture a clear particle profile. The source's light could pass through the entire measurement section. The time-series images of the particle motion field in a two-dimensional oil stream were recorded using a CMOS camera. The camera captured 210 images per second at full resolution. Due to the small diameter of the wear particles, a magnifying objective lens of 2× was attached to the front of the camera. After calibration, the field of view was limited to 8 mm × 6 mm, and the camera resolution was 4 μm/pixel. In addition, the particle velocity was calculated using the ECO algorithm in the next section, and the time interval depended on the CMOS frame rate. Streampix software was used to record the videos, and it could be used to change many important photographic parameters (such as the recording time, exposure time, and shooting rate).
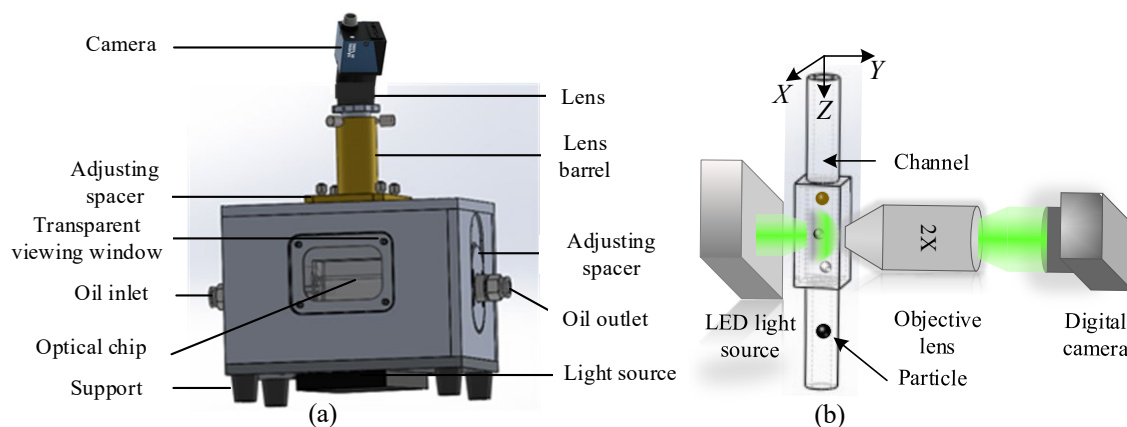

Figure 13. (**a**) Three-dimensional model of the particle monitoring sensor. (**b**) Schematic of sensor.

In addition, the choice of measurement section had a significant influence on the calculation results, and the image of the near-wall area of the circular pipe was distorted by the optical lens, which reduced the identification of particles in the near-wall area. At the same time, since the visible area was too small to reflect the real flow field, a custom-designed flow channel for inline flow was used, as illustrated in Figure 13b. The specific principle was that a 5-cm long rectangular oil-filled sleeve was attached to the outside of the circular pipe in the measurement section, to prevent distortion of the visual image. In addition, the viewport was made of highly-transparent quartz glass with good corrosion resistance.

3.4. Experimental Study Results

3.4.1. Velocity Measurement of the Particles

As images of solid particles in liquid–solid two-phase flows are subject to interference from the liquid environment, they can suffer from morphological changes, image blurring, and other disturbances, and the motion tracking of particles can be greatly affected. This paper introduced the robust ECO tracking algorithm for the tracking and velocity measurement of wear particles in a full-flow inline environment. The ECO algorithm mainly consists of steps such as a correlation filter and efficient convolution operation, and it was implemented in the Python environment.

(a) The principle of the correlation filter is shown in Figure 14: first, the similarity between the selected filter and the input image was calculated, to obtain the correlation function. The larger the value, the higher the correlation. When the value reached the maximum, the image of the tracking target could be determined, and then the filter was continuously updated using an inverse Fourier transform method.
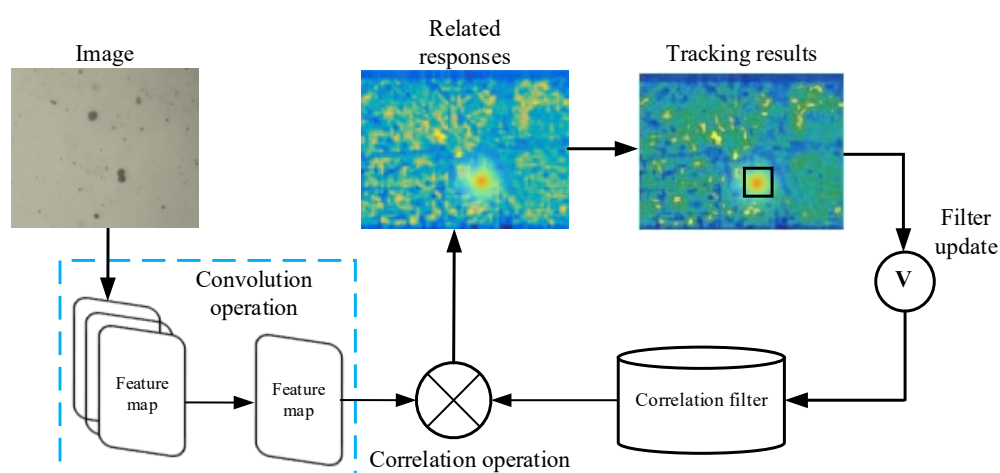
Figure 14. Schematic diagram of the tracking method based on a correlation filter.

(b) For efficient convolution operation, the response function was obtained by first extracting the feature function of the input image using the resolution and combining it with the constantly updated filter. Then a matrix was created, to convolve the feature map based on the feature contribution, thereby reducing the dimensionality of the feature map. The final result was the continuous tracking of the target.

3.4.2. Experimental System

The experiments were carried out in the Key Laboratory of Civil Aviation Health Monitoring and Intelligent Maintenance at Nanjing University of Aeronautics and Astronautics. The experimental system is shown in Figure 15, which included a MMW-1A pin-disk test rig (particle generator), a self-made full-flow inline optical monitoring sensor, a manual oil pump, an oil storage tube, and other components. Above the oil inlet of the full-flow inline optical sensor, there was a vertical transparent acrylic pipe with a test part under the ball valve 1. The length was 300 mm, which provided a long enough distance for the particles' vertical movement, so that the particles' velocities passing the sensor reached stability. The inner diameter of the vertical pipe was 8 mm. The oil sample used in the equipment was No. 26 industrial white oil. In accordance with the materials commonly used in engines in [14], the ball test piece of the pin-disk friction and wear test machine was made of bearing steel. Three types of materials were used for the disc test piece: copper, titanium, and nylon of high, medium, and low density; the parameters are shown in Table 2, and the detailed internal structure of the pin-on-disk was described in a previous study [14].
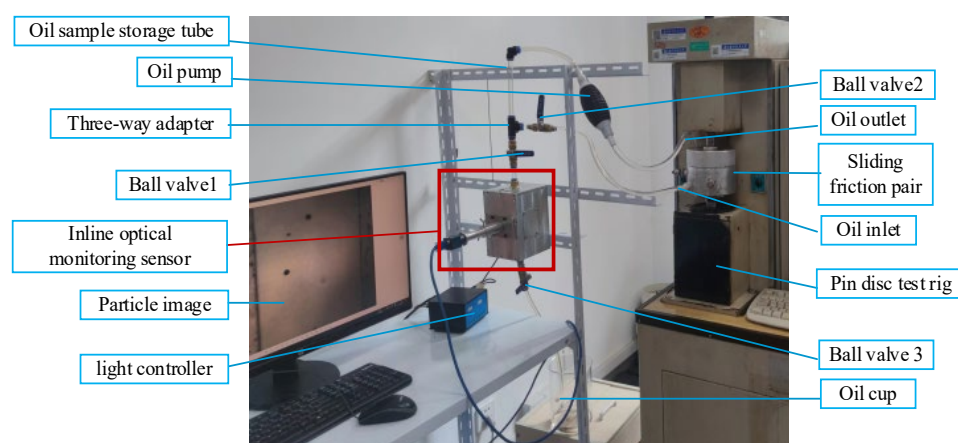

**Figure 15.** Inline monitoring sensor installed on a pin-disk test rig.

Table 2. The material of the test piece of the disc.

Test Material	Copper	Titanium	Nylon
Density (kg/m³)	8900	4500	1150

Before starting the experiment, the entire experimental pipeline was filled with oil, and then the ball valve 1, ball valve 2, and ball valve 3 were closed, and the load of the pin-disk friction and wear tester was set to 300 N. After it had worked for 5 h, ball valve 2 was opened, and the oil pump was manually kneaded ten times to make the oil sample carrying particles in the pin plate mix evenly in the whole pipeline, then ball valve 2 was closed. After the oil sample had been stationary for 10 min, ball valve 1 was opened, the full flow inline optical sensor was opened, and the solid particles were injected into the dead oil. This ensured that the particles had no initial velocity in the oil and the falling velocity of a single particle was zero when it entered the monitoring sensor. It then became constant due to the action of gravity, drag force, and buoyancy. The bearing steel ball specimen and disc specimen were replaced. Five measurements were performed for each experiment, to eliminate experimental random error, and the particle velocity was finally averaged. After all the experiments were completed, ball valve 3 was open, and the oil in the pipeline flowed into the oil cup.

3.4.3. Experimental Results

In the experiment, the motion of a copper particle from its appearance in the sensor field of view to its departure was recorded, as shown in Figure 16, and the camera captured a total of 11 photographs. It can be seen that the wear particles moved gradually towards the center in the *Y*-direction of the transparent pipe and moved with the same displacement in the *Z*-direction at the same time interval, so the velocity of the wear particles had reached stability. Their velocity vector no longer varied with time, which also proved the correctness of the simulation. We could calculate the diameter of the particles by the size of the pixel area they occupied ($d_P = \sqrt{4S/\pi}$). Then the different particle velocities could be calculated using the ECO tracking velocimetry algorithm. In addition, it can also be seen that, in the experiments, certain irregularly shaped particles did not move along the center of the pipe. The reason for this was that the surface roughness of irregularly shaped particles was not considered in the previous theoretical analysis and simulation. At the same size, the rougher the particle surface, the greater the flow field effect on the particle surface. Due to the irregular shape of the wear particles, the flow resistance and the gravity of the particles were not in the same line, which led to an unbalanced combined force on the particles, so several particles were not in the center of the pipe.
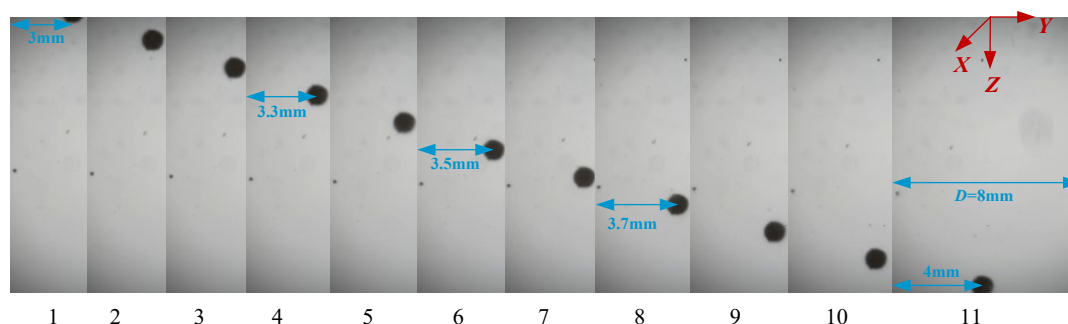
Figure 16. The process of a spherical copper particle from appearing in the sensor field of view to leaving.

3.4.4. Monitoring Model

The velocities of all the particles monitored by the sensors in the experiment and the curve fitted to their trends are shown in Figure 17. We can see that the overall velocity of

particle movement increased with increasing particle size. For the same particle size, the greater the density of the particles, the greater the velocity of movement, which was consistent with the theoretical calculations and simulations. At the same time, the smaller diameter particles made up a larger proportion, which was also in line with the wear curve pattern of the equipment in Figure 3. The polynomial function was used to fit the velocity points of the different densities of particles separately. The R^2 showed that the regression equations of all three fitted curves had a high degree of fit (the closer the R^2 is to 1, the better the fitted curve fits the original data [20]), indicating that these three curves could be used as a monitoring model for these three typical densities of particles in this sensor. In this model, since the diameter of the particles can be directly observed using the inline optical monitoring sensor designed in this paper, and as the velocity of the particles can be obtained through the particle velocimetry algorithm, a rough value of the particle density can be obtained with the monitoring model.
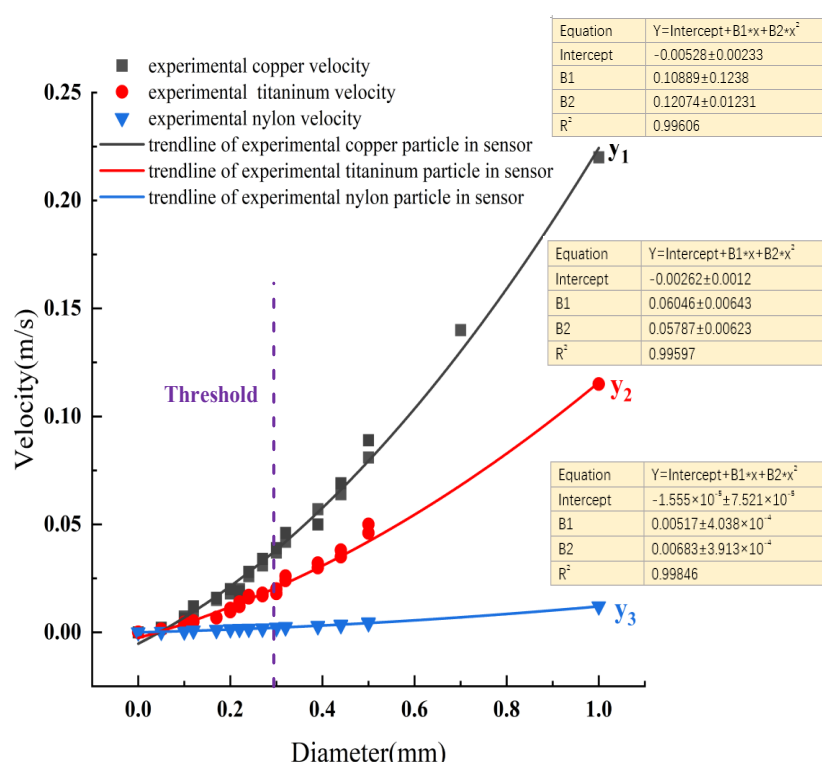

Equation	$Y=Intercept+B1*x+B2*x^2$
Intercept	-0.00528 ± 0.00233
B1	0.10889 ± 0.1238
B2	0.12074 ± 0.01231
R^2	0.99606

Equation	$Y=Intercept+B1*x+B2*x^2$
Intercept	-0.00262 ± 0.0012
B1	0.06046 ± 0.00643
B2	0.05787 ± 0.00623
R^2	0.99597

Equation	$Y=Intercept+B1*x+B2*x^2$
Intercept	$-1.555\times10^{-5}\pm7.521\times10^{-5}$
B1	$0.00517\pm4.038\times10^{-4}$
B2	$0.00683\pm3.913\times10^{-4}$
R^2	0.99846

Figure 17. Velocities of particles with different properties, and their fitting curves in the experiment.

It can be seen that there was a high degree of agreement between the experimental and model fitting results for particles below 300 μm in diameter, while as the particle diameter became larger, the error became larger. Hence, we set the monitoring threshold to 300 μm, and according to the particle's velocity and diameter, the density of the particles could be directly obtained, so that the wear parts could be accurately obtained. Meanwhile, from the wear law of mechanical equipment in Figure 3, it can be seen that when the particle diameter is greater than 300 μm, a catastrophic accident will occur in the equipment. Therefore, the sensor and monitoring model can be effectively used for inline wear monitoring of the equipment.

3.5. Discussion

We verified the theoretical calculations and simulations analyses step by step, to determine the feasibility of identifying the properties of wear particles based on their motion characteristics. Then, an inline optical detection sensor was designed to monitor the particles generated by the wear of rotating parts in real time in the oil line. When the particle

size is larger than 300 μm, the system will raise an alarm for the engineer. The above experiments clearly confirmed that the designed inline optical particle monitoring sensor is able to monitor the appearance of particles with good sensitivity and in real time. Compared to conventional ferrography [9,16–18], this method avoided aggregating many ferromagnetic particles into chains due to magnet adsorption. It improves the efficiency of individual wear particle identification. Instead of other microfluidic optical sensors for offline monitoring [14,20], we used inline monitoring for full-flow real-time monitoring of wear particles, with the advantages of no sampling, being real-time, and no human intervention. In addition to considering simple spherical wear particles and ferromagnetic particles, we also simulated the motion of other typical shapes and particle densities. Therefore, the proposed method and the designed sensor in this paper are of great significance for the monitoring of rotating machinery.

4. Conclusions

In order to monitor the wear particles appearing in a lubricating oil pipeline in real-time, this paper designed and processed a lubricating oil wear particle inline monitoring sensor based on theoretical analysis and simulation research, which mainly consists of a camera, telecentric lens, LED light source, rectangular oil sleeve to prevent image distortion, and target tracking speed measurement algorithm. The sensor can monitor the diameter and density of micro-sized particles in the inline oil pipe, and the following conclusions were drawn:

(1) Utilizing the characteristics of the wear particles monitored by the sensor, an ECO-based target tracking velocity measurement algorithm was developed. The experimental results showed that it has a good robustness.

(2) The velocities of wear particles within the self-developed sensor were divided into an acceleration section at the beginning and a later uniform velocity section. However, the acceleration time was within 0.1 s. Furthermore, the uniform velocity was positively correlated with the particle size and density, but not linearly. The greater the particle density, the greater the final stabilization velocity. The larger the particle diameter, the greater the final stabilization velocity. As demonstrated experimentally, the stabilization velocity of the particle was related to its circularity. The more round the particles were, the higher the velocity after stabilization. Notably, the initial position of the wear particle had no significant effect on the final stabilization position and the velocity in the sensor.

(3) The number of particles with diameters less than 300 μm observed in the experiment was large. The data model fitting results were compared with multiple sets of experimental results monitored by the inline sensor. The results showed that the model had a better fitting effect with wear particles of different densities, and the R^2 values were all larger than 99%. The distribution range of the particle diameter conforms to the particle generation law of rotating equipment, so 300 μm was used as the monitoring threshold for the sensor. When the threshold is exceeded, monitoring information will be sent to the engineer, and the severe wear area will be judged according to the abrasive particle density.

This research showed that an inline method, based on wear particle velocity analysis, for monitoring wear particles is feasible for practical applications in lubricant monitoring and could have some industrial applications. Moreover, the inline optical sensor studied in this paper contributes to speeding up the visualization process in the monitoring and diagnostic process of the operating status of rotating machines in SCADA (Supervisory Control and Data Acquisition) systems. Since the inline optical monitoring method proposed in this paper has the advantages of no sampling, being real-time, and no human intervention, oil monitoring techniques are greatly improved. Future work including particle roughness factors and the effect of irregular shaped of particles will be added to subsequent calculations and simulations, to obtain more accurate particle movement monitoring results. Furthermore, a comprehensive 3D data model will be established, to monitor the properties of wear particles in real-time, based on a large amount of experimental

data. At the same time, after the practical application of this monitoring system, a monitoring model considering other properties of the oil and the velocity of wear particles will be developed. Finally, the ability to inline monitor mechanical equipment failures could be greatly improved.

Nomenclature

Symbol	Unit	Description
d_p	μm	Particle size
g	m/s^2	Gravitational acceleration
D	μm	Pipe diameter
L	μm	Pipe length
ρ_p	kg/m^3	Particle density
ρ_f	kg/m^3	Oil density
ζ	/	Drag coefficient
u_p	m/s	Particle movement velocity
u_{pt}	m/s	Free settling velocity of a single solid sphere in an unbounded fluid
u_f	m/s	Fluid flow rate
ϑ	m^2/s	Kinematic viscosity coefficient of oil
μ	N $\cdot$ s/m^2	Dynamic viscosity coefficient of oil
t, τ	s	Time
F_g	N	Gravity
F_f	N	Buoyancy
F_D	N	Drag force
F_M	N	Additional mass force
F_B	N	Basset force
F_S	N	Saffman lifting force
Re_p	/	Particle Reynolds number
u'_p	m/s	Particle movement velocity
P	Pa	Pressure
u_x, u_y, u_z	m/s	The velocity component of the fluid at time t in the x, y, z direction
f_x, f_y, f_z	m/s	The external force per unit volume of fluid in the x, y, z direction
S	μm^2	Particle image pixel area
e	/	Circularity of particle

References

1. Lu, P.; Powrie, H.E.; Wood, R.J.K.; Harvey, T.J.; Harris, N.R. Early wear detection and its significance for condition monitoring. *Tribol. Int.* **2021**, *159*, 106946. https://doi.org/10.1016/j.triboint.2021.106946.

2. Li, D.; Zhang, M.; Kang, T.; Li, B.; Xiang, H.; Wang, K.; Pei, Z.; Tang, X.; Wang, P. Fault diagnosis of rotating machinery based on dual convolutional-capsule network (DC-CN). *Measurement* **2022**, *187*, 110258. https://doi.org/10.1016/j.measurement.2021.110258.

3. Li, Y.; Zou, W.; Jiang, L. Fault diagnosis of rotating machinery based on combination of Wasserstein generative adversarial networks and long short term memory fully convolutional network. *Measurement* **2022**, *191*, 110826. https://doi.org/10.1016/j.measurement.2022.110826.

4. Ravikumar, K.N.; Yadav, A.; Kumar, H.; Gangadharan, K.V.; Narasimhadhan, A.V. Gearbox fault diagnosis based on Multi-Scale deep residual learning and stacked LSTM model. *Measurement* **2021**, *186*, 110099. https://doi.org/10.1016/j.measurement.2021.110099.

5. Tang, M.; Liao, Y.; He, D.; Duan, R.; Zhang, X. Rolling bearing diagnosis based on an unbiased-autocorrelation morphological filter method. *Measurement* **2022**, *189*, 110617. https://doi.org/10.1016/j.measurement.2021.110617.

6. Tao, L.; Sun, L.; Wu, Y.; Lu, C.; Ma, J.; Cheng, Y.; Suo, M. Multi-signal fusion diagnosis of gearbox based on minimum Bayesian risk reclassification and adaptive weighting. *Measurement* **2022**, *187*, 110358. https://doi.org/10.1016/j.measurement.2021.110358.

7. Yao, Y.; Gui, G.; Yang, S.; Zhang, S. An adaptive anti-noise network with recursive attention mechanism for gear fault diagnosis in real-industrial noise environment condition. *Measurement* **2021**, *186*, 110169. https://doi.org/10.1016/j.measurement.2021.110169.

8. Cheng, C.; Ma, G.; Zhang, Y.; Sun, M.; Teng, F.; Ding, H.; Yuan, Y. A Deep Learning-Based Remaining Useful Life Prediction Approach for Bearings. *IEEE/ASME Trans. Mechatron.* **2020**, *25*, 1243–1254. https://doi.org/10.1109/tmech.2020.2971503.

9. Wang, J.; Wang, G.; Cheng, L. Texture extraction of wear particles based on improved random Hough transform and visual saliency. *Eng. Fail. Anal.* **2020**, *109*, 104299. https://doi.org/10.1016/j.engfailanal.2019.104299.

10. Hong, W.; Cai, W.; Wang, S.; Tomovic, M.M. Mechanical wear debris feature, detection, and diagnosis: A review. *Chin. J. Aeronaut.* **2018**, *31*, 867–882. https://doi.org/10.1016/j.cja.2017.11.016.

11. Liu, R.; Bei, S.; Gu, M.; Wang, H.; Sun, J. Research on Characteristics of Electrostatic Wear-Site and Oil-Line Sensor with Theoretical and Comprehensive Analysis. *J. Sens.* **2022**, *2022*, 9188776. https://doi.org/10.1155/2022/9188776.

12. Guerrero, J.M.; Castilla, A.E.; Fernandez, J.A.S.; Platero, C.A. Transformer Oil Diagnosis Based on a Capacitive Sensor Frequency Response Analysis. *IEEE Access* **2021**, *9*, 7576–7585. https://doi.org/10.1109/access.2021.3049192.

13. Yu, B.; Cao, N.; Zhang, T. A novel signature extracting approach for inductive oil debris sensors based on symplectic geometry mode decomposition. *Measurement* **2021**, *185*, 110056. https://doi.org/10.1016/j.measurement.2021.110056.

14. Liu, Z.; Liu, Y.; Zuo, H.; Wang, H.; Wang, C. Oil debris and viscosity monitoring using optical measurement based on Response Surface Methodology. *Measurement* **2022**, *195*, 111152. https://doi.org/10.1016/j.measurement.2022.111152.

15. Jia, R.; Wang, L.; Zheng, C.; Chen, T. Online Wear Particle Detection Sensors for Wear Monitoring of Mechanical Equipment—A Review. *IEEE Sens. J.* **2022**, *22*, 2930–2947. https://doi.org/10.1109/jsen.2021.3131467.

16. Fan, H.; Gao, S.; Zhang, X.; Cao, X.; Ma, H.; Liu, Q. Intelligent Recognition of Ferrographic Images Combining Optimal CNN with Transfer Learning Introducing Virtual Images. *IEEE Access* **2020**, *8*, 137074–137093. https://doi.org/10.1109/access.2020.3011728.

17. Wang, J.; Bi, J.; Wang, L.; Wang, X. A non-reference evaluation method for edge detection of wear particles in ferrograph images. *Mech. Syst. Signal Processing* **2018**, *100*, 863–876. https://doi.org/10.1016/j.ymssp.2017.08.014.

18. Feng, S.; Qiu, G.; Luo, J.; Han, L.; Mao, J.; Zhang, Y. A Wear Debris Segmentation Method for Direct Reflection Online Visual Ferrography. *Sensors* **2019**, *19*, 723. https://doi.org/10.3390/s19030723.

19. Wu, T.; Wu, H.; Du, Y.; Peng, Z. Progress and trend of sensor technology for on-line oil monitoring. *Sci. China Technol. Sci.* **2013**, *56*, 2914–2926. https://doi.org/10.1007/s11431-013-5400-5.

20. Liu, Z.; Liu, Y.; Zuo, H.; Wang, H.; Fei, H. A Lubricating Oil Condition Monitoring System Based on Wear Particle Kinematic Analysis in Microfluid for Intelligent Aeroengine. *Micromachines* **2021**, *12*, 748. https://doi.org/10.3390/mi12070748.

21. Peng, Y.; Wu, T.; Wang, S.; Du, Y.; Kwok, N.; Peng, Z. A microfluidic device for three-dimensional wear debris imaging in online condition monitoring. *Proc. Inst. Mech.Eng. Part J J. Eng. Tribol.* **2016**, *231*, 965–974. https://doi.org/10.1177/1350650116684707.

22. Feng, S.; Zeng, Q.H.; Fan, B.; Luo, J.F.; Xiao, H.; Mao, J.H. Wear Debris Segmentation of Reflection Ferrograms Using Lightweight Residual U-Net. *IEEE Trans. Instrum. Meas.* **2021**, *70*, 3099573. https://doi.org/10.1109/tim.2021.3099573.

23. Peng, P.; Wang, J.G. FECNN: A promising model for wear particle recognition. *Wear* **2019**, *432*, 202968. https://doi.org/10.1016/j.wear.2019.202968.

24. Segré, G.; Silberberg, A. Behaviour of macroscopic rigid spheres in Poiseuille flow Part 2. Experimental results and interpretation. *J. Fluid Mech.* **2006**, *14*, 136–157. https://doi.org/10.1017/s0022112062001111.

25. Jeffrey, R.C.; Pearson, J.R.A. Particle motion in laminar vertical tube flow. *J. Fluid Mech.* **2006**, *22*, 721–735. https://doi.org/10.1017/s0022112065001106.

26. Shehua, H.; Wei, L.; Liangjun, C. On equation of discrete solid particles' motion in arbitrary flow field and its properties. *Appl. Math. Mech.* **2000**, *21*, 297. https://doi.org/10.1007/BF02459008.

27. Choi, H.M.; Kurihara, T.; Monji, H.; Matsui, G. Measurement of particle/bubble motion and turbulence around it by hybrid PIV. *Flow Meas. Instrum.* **2002**, *12*, 421–428. https://doi.org/10.1016/S0955-5986(01)00030-9.

28. Miura, K.; Itano, T.; Sugihara-Seki, M. Inertial migration of neutrally buoyant spheres in a pressure-driven flow through square channels. *J. Fluid Mech.* **2014**, *749*, 320–330. https://doi.org/10.1017/jfm.2014.232.

29. Oseen, C.W. *Neuere Methoden Und Ergebnisse in Der Hydrodynamik*; Akademische Verlagsgesellschaft: Leipzig, Germany, 1927.

30. Barton, I.E. Computation of particle tracks over a backward-facing step. *J. Aerosol Sci.* **1995**, *26*, 887–901. https://doi.org/10.1016/0021-8502(95)00018-8.

31. Fan, L.; Zhu, C. Momentum Transfer and Charge Transfer. In *Principles of Gas-Solid Flows*; Cambridge Series in Chemical Engineering; Cambridge University Press: Cambridge, UK, 1998; pp. 87–129.

32. Hedayati Nasab, S. Free Falling of Spheres in a Quiescent Fluid, 2017. Available online: https://spectrum.library.concordia.ca/id/eprint/983050/ (accessed on 1 September 2021).

33. Sun, J.; Wang, L.; Li, J.; Li, F.; Li, J.; Lu, H. Online oil debris monitoring of rotating machinery: A detailed review of more than three decades. *Mech. Syst. Signal Processing* **2021**, *149*, 107341. https://doi.org/10.1016/j.ymssp.2020.107341.

34. Yang, X. *The Motion of the Particles in Simple Flows Using the Lattice Boltzmann Method*; University of Science and Technology of China: Hefei, China, 2016.

35. Aidun, C.K.; Lu, Y.; Ding, E.J. Direct analysis of particulate suspensions with inertia using the discrete Boltzmann equation. *J. Fluid Mech.* **1998**, *373*, 287–311. https://doi.org/10.1017/S0022112098002493.

36. Peng, P.; Wang, J. Wear particle classification considering particle overlapping. *Wear* **2019**, *422–423*, 119–127. https://doi.org/10.1016/j.wear.2019.01.060.